JOURNAL OF SOLID STATE CHEMISTRY **141,** 199–204 (1998)
ARTICLE NO. SC987951

On the Crystal Structure of Fe_6Ge_5 and Its Relationship to *B*8-Type Structures

Ann-Kristin Larsson,*,[1] Sigrid Furuseth,† and Ray Withers*

*Research School of Chemistry, Australian National University, Canberra, ACT, 0200 Australia; and †Department of Chemistry, University of Oslo, N-0315 Oslo 3, Norway

Received July 2, 1997; in revised form June 29, 1998; accepted July 1, 1998

Epitaxial intergrowths of Fe_6Ge_5 and *B*8-type $Fe_{1+x}Ge$ was investigated by means of electron diffraction. A crystal structure description of Fe_6Ge_5 in terms of *B*8- and *B*1-type structures was established; 4/5 of the Ge atoms in Fe_6Ge_5 can be described with one-octahedron wide slabs of hexagonal close-packed Ge atoms with all octahedral sites and 1/2 of the trigonal bipyramidal sites therein filled with Fe atoms (*B*8). Additionally, all Ge atoms can be described by a two-octahedra wide slab of cubic close-packed Ge atoms with 4/6 of the octahedral sites filled with Fe atoms and 1/6 of the octahedral sites filled with *two* Fe atoms, one in each square pyramid (*B*1). At the surface interconnecting these slabs, octahedra from the *B*8 and *B*1 slabs share faces and the trigonal bipyramid from the hcp array and two edge-sharing tetrahedra from the ccp array are merged to form a pentagonal bipyramid.

INTRODUCTION

In the Fe–Ge phase diagram (1), three phases are known to exist within the composition range $Fe_{1+x}Ge$, $0 < x < 1$. The η ($0.29 < x < 0.39$ at 700°C) and β ($0.5 < x < 0.74$ at 700°C) phase fields have been reported as being of NiAs–Ni_2In (*B*8) type or a modulated variant there of (2–6), while Fe_6Ge_5 ($x = 0.2$) is reported as having its own distinct structure type (isostructural to Fe_6Ga_5 (7)).

Intermetallic $T_{1+x}B$, $0 < x < 1$, phases, where T is a transition metal and B is a metal or semimetal from group III*B*–VI*B* frequently adopt the NiAs–Ni_2In (*B*8) type structure ($P6_3/mmc$ space group symmetry, $a \approx 4$ and $c \approx 5$ Å). In these intermetallic *B*8-type structures, the hcp array of B atoms is compressed about 25% along the c axis, all the octahedral sites are filled by T atoms, and a fraction, x, of the trigonal bipyramidal sites are filled with additional T atoms.

Ordering of the additional T atoms on these trigonal bipyramidal sites very often gives rise to additional features in reciprocal space, readily revealed by electron diffraction (ED) (8). These additional diffraction features range from weak diffuse scattering, via strongly localized diffuse scattering, to sharp additional satellite reflections. Only commensurately modulated superstructures that metrically distort to a significant extent the underlying *B*8 hexagonal subcell lattice parameters (to orthorhombic, monoclinic, or triclinic) can easily be identified by routine XRD methods. At the other extreme, if the strain distortion of the underlying *B*8 hexagonal subcell lattice parameters is large and the superstructure reflections are very strong, the connection to the *B*8-type structure may not be at all obvious.

Fe_6Ge_5 has a composition that results in a *B*8-type structure for many T–B systems, but the reported crystal structure of Fe_6Ge_5 is *not* a simple superstructure of the *B*8 type. Driven by the question why this structure was not of *B*8 type, our initial intention was to explore the connection between the Fe_6Ge_5 and *B*8-type phases. ED was employed as a tool to effectively study real and reciprocal space relationships simultaneously and at the same time record any twinning emphasizing structure motifs. It became obvious during ED investigation that the crystal structure relationship between the two phase types is very real and goes much further than only formal connections for descriptive purposes. This was manifested experimentally in the frequent occurrence of epitaxial intergrowths of the *B*8- and the Fe_6Ge_5-type phases.

The crystal structure of Fe_6Ge_5 was refined by Malaman *et al.* (7) and described in terms of nets and compared to the *B*35-type structure (the CoSn-type structure of FeGe). It was also mentioned that structure motifs similar to $Ni_{13}Ga_9$ (which is a superstructure of *B*8 type) were present in the structure. In this contribution we will describe the structure in terms of coordination polyhedra of Ge atoms around the Fe atoms and from that compare the polyhedral arrangement in Fe_6Ge_5 to that of a *B*8-type (super) structure and to the *B*1- (NaCl) type structure.

[1]To whom correspondence should be addressed. Present address: Inorganic Chemistry, Arrhenius Laboratory, 106 91 Stockholm, Sweden.

0022-4596/98 $25.00

EXPERIMENTAL

Weighed amounts of Fe and Ge of nominal composition Fe_6Ge_5 were heated in alumina crucibles enclosed in evacuated silica tubes at 800°C for 1 week. The resulting ingot was then crushed and annealed at 400°C for a further month. The sample resulting from this process was nonetheless still multiphase. Most of the iron-rich crystallites were removed from this sample via the use of a magnet. (The NiAs–Ni_2In type η and β phases and the more Fe-rich compounds in the Fe–Ge system are ferromagnetic (2, 3).) To avoid unnecessary contamination of the JEOL 100CX Transition Electron Microscope (TEM) used to record the electron diffraction patterns (EDP's), some further Ge was added to the sample studied most intensely. The nominal composition was thereby changed to $Fe_{1.14}Ge$ and the sample was reannealed at 550°C for 4 weeks.

The phase composition of the samples was monitored by PXRD using a Guinier–Hägg camera with Cu$K\alpha_1$ radiation (dark background caused by fluorescence). Si (NBS No. 640) was added as an internal standard for the determination of unit-cell dimensions. The specimens for the TEM were prepared by crushing and dispersing onto holey carbon-coated copper grids.

RESULTS

The Relationship between the B8 and the Fe_6Ge_5 Reciprocal Lattices

In the multiphase sample annealed at 400°C, single grains containing both the Fe_6Ge_5 phase and a (short-range ordered) *B*8-type phase were frequently found during TEM investigation. By moving the beam from one side of such grains to the other and studying the change in the EDPs obtained, it was concluded that the two phases present were growing epitaxially on each other. For example, on moving the beam about on a grain oriented along a $\langle 100\rangle_{B8}$ zone axis, it was sometimes noticed that the $h0l$, $l = 2n + 1$ reflections of the *B*8-type structure could be made to vanish, while reflections corresponding to $h0l$, $l = 2n$ remained strong. At the same time, strong "satellite" reflections corresponding to a primary modulation wave vector $\mathbf{q} = 1/4\ [1\,0\,\bar{1}\,4]^*$ appeared around the remaining Bragg reflections (see Fig. 1a). (Note that reflection indices and zone axes with the subscript "*B*8" refer throughout the paper to the $P6_3/mmc$, *B*8-type cell, $a \approx 4.0$, $c \approx 5.0$ Å, and with the subscript "m" to the monoclinic cell of Fe_6Ge_5.) This new diffraction pattern corresponds to the $[0\,1\,0]_m$ zone axis of the Fe_6Ge_5 phase. The $h0l$, $l = 2n$-type reflections remaining from the *B*8-type lattice are emphasized by circles in the figure.

In the same way, the EDP characteristic of the *B*8 structure when oriented along the $[0\,0\,1]_{B8}$ zone axis was observed to change to the EDP of Fig. 1b (corresponding to

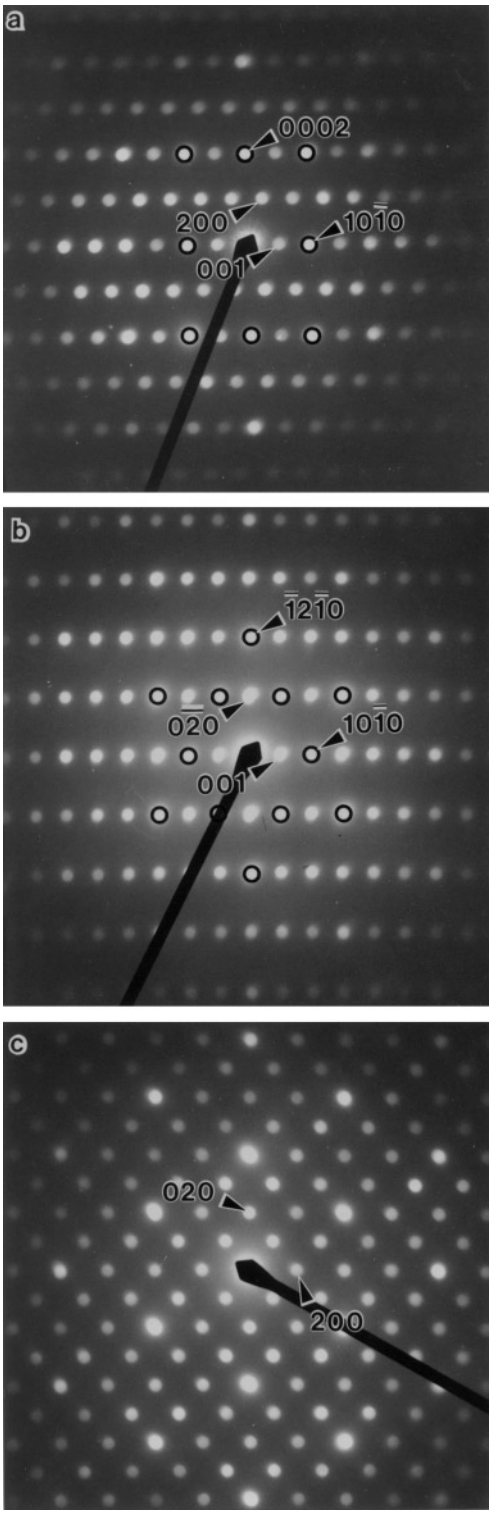

FIG. 1. EDPs from the three major zone axes of Fe_6Ge_5. (a) is along $\langle 010\rangle_m$ and (b) is along $\langle 100\rangle_m$, corresponding to $\langle 100\rangle_{B8}$ and $\langle 001\rangle_{B8}$, respectively. These two EDP are indexed in both the $P6_3/mmc$ *B*8-type structure (four index) and the monoclinic Fe_6Ge_5 type structure. Reflections of the *B*8-type sublattice are circled as a guide for the eye. (c) is along $\langle 001\rangle_m$, which does not correspond to a major zone axis in the *B*8-type structure.

the $[100]_m$ zone axis of the Fe_6Ge_5 phase) on movement of the electron beam across a single grain. Again the reflections of the corresponding *B*8-type lattice (i.e., *hk*0-type reflections) are circled. The third major zone axis of Fe_6Ge_5, $[001]_m$ corresponds to a minor zone axis in the *B*8-type structure, $[42\bar{6}\bar{1}]_{B8}$ (Fig. 1c). The similarities between the $\langle 010\rangle_m$ and the $\langle 100\rangle_{B8}$ zone axis EDPs and the $\langle 100\rangle_m$ and the $\langle 001\rangle_{B8}$ zone axis EDPs together with the fact that the two types of crystallites intergrow epitaxially indicate that it is possible to describe the reciprocal cell of Fe_6Ge_5 in terms of the reciprocal lattice parameters of a *B*8-type lattice and vice versa. This reciprocal space relationship is given by $\mathbf{a}_m^* = 1/8[10\bar{1}4]_{B8}^*$, $\mathbf{b}_m^* = 1/4[1\bar{2}10]_{B8}^*$, and $\mathbf{c}_m^* = 1/2[10\bar{1}0]_{B8}^*$. The corresponding real space relationship is $\mathbf{a}_m = 2\mathbf{c}_{B8}$, $\mathbf{b}_m = -2\mathbf{b}_{B8}$ and $\mathbf{c}_m = 2\mathbf{a}_{B8} + \mathbf{b}_{B8} - 1/2\mathbf{c}_{B8}$.

The cell reported by Malaman *et al.* (7), *C*2/*m*, $a = 9.965$ Å, $b = 7.826$ Å, $c = 7.801$ Å, and $\beta = 109.67°$ thus corresponds to a distorted *B*8-type subcell with $c_{B8} = a/2 = 4.983$ Å, $b_{B8} = b/2 = 3.913$ Å, and $a_{B8} = 1/8|[124]_m| = |\mathbf{a}_{B8} + \mathbf{b}_{B8}| = 1/8|[1\bar{2}4]_m| = 4.162$ Å. There is clearly a relatively strong monoclinic, but pseudo-orthorhombic, distortion of the *B*8 subcell (compare Fig. 1b). The very close to 2*mm* projection symmetry of Figs. 1a and 1b shows that Fe_6Ge_5 very nearly possesses orthorhombic *mmm* diffraction symmetry. The true space group symmetry, however, is not orthorhombic but monoclinic *C*2/*m* (7) (*vide infra*).

An alternative way to describe the set of Bragg reflections from the Fe_6Ge_5 phase is as $\mathbf{H} = \mathbf{G}_s \pm m\mathbf{q}$, where $\mathbf{G}_s$ represents the set of Bragg reflections that the Fe_6Ge_5 and *B*8-type phases have in common (i.e., the reflections characteristic of the *B*8-type structure with the additional condition that reflections *hkl* occur only for $l = 2n$ (see Fig. 1a)), $\mathbf{q}$ is a primary modulation wave vector given by $\mathbf{q} = 1/8[3\bar{4}14]_{B8}^*$ (see Fig. 2), and *m* is an integer. In Fig. 2a, an EDP of the

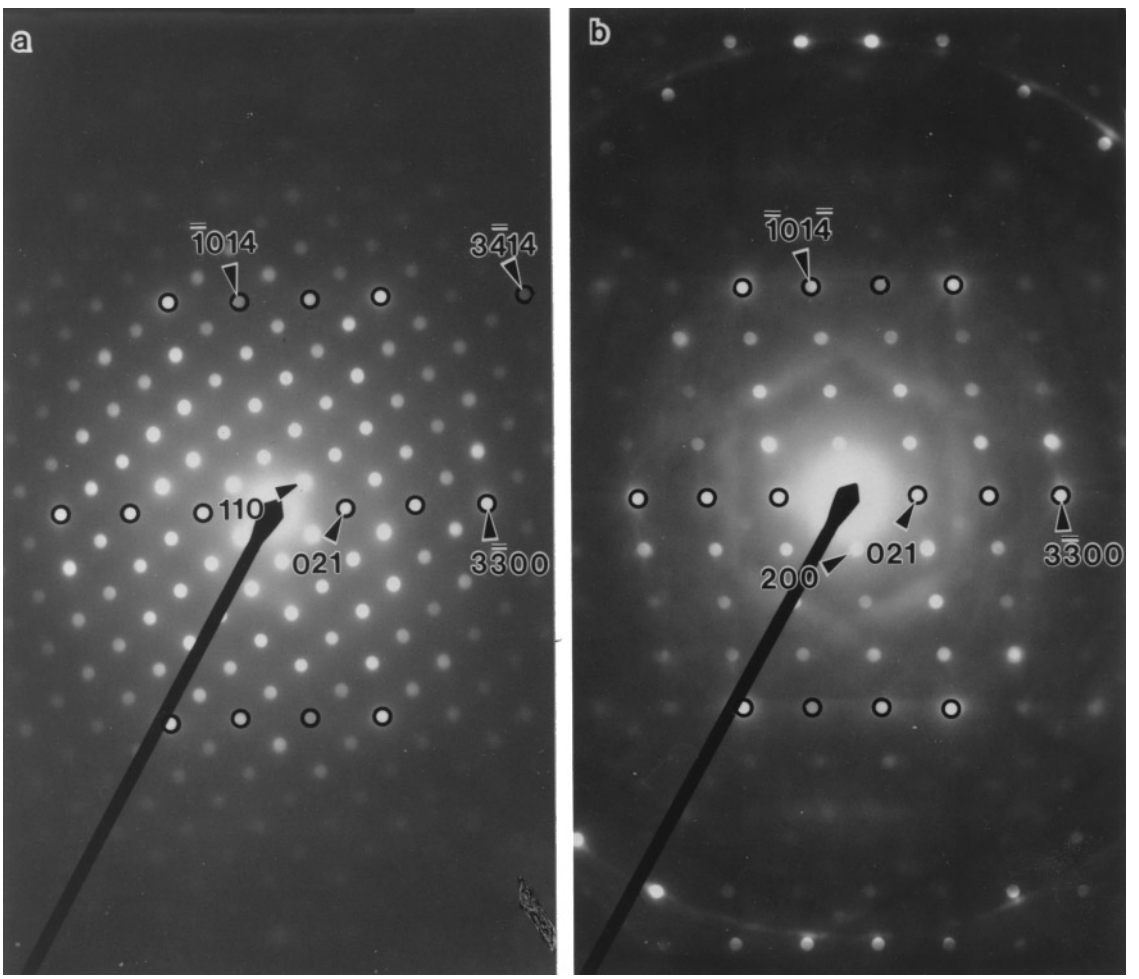

FIG. 2. EDPs from two zone axes of Fe_6Ge_5 corresponding to two $\langle 401\rangle_{B8}$ symmetry related zone axis of the *B*8-type structure. (a) is along the zone axis $\langle 1\bar{1}2\rangle_m = [441]_{B8}$ (according to the orientation of the *B*8 lattice given by the transformation matrix in the text) and (b) is along $\langle 01\bar{2}\rangle_m = [44\bar{1}]_{B8}$. These two EDP are indexed in both the $P6_3/mmc$ *B*8-type structure (four index) and the monoclinic Fe_6Ge_5 type structure. Reflections of the *B*8-type sublattice are circled as a guide for the eye. These EDPs, recorded from different domains of a domain twinned grain (without tilting the specimen), clearly demonstrate that the connections between the structures go further than the cell parameters. Note in (a) how all reflections of the Fe_6Ge_5 phase can be indexed with $\langle hk2l\rangle_{B8*} + 1/8\langle 3\bar{4}14\rangle_{B8*}$.

zone axis $[1\bar{1}2]_m = [441]_{B8}$ is shown. The circled reflections can be indexed according to the $P6_3/mmc$ *B*8-type structure (indicated by four indices) and all reflections can be indexed as $\mathbf{G}_{B8} + m\mathbf{q}$ where $\mathbf{q} = 1/8[3\bar{4}14]^*_{B8}$, (in the EDP of this projection $\mathbf{G}_{B8} \in \mathbf{G}_s$).

The EDPs in Fig. 2 are from a twinned crystallite (7) of the $Fe_{1.14}Ge$ sample. The EDP in Fig. 2b (zone axis $[0\bar{1}2]_m = [44\bar{1}]_{B8}$) is recorded from a different part of the same grain as the EDP in Fig. 2a without tilting the specimen. Note that $[441]_{B8}$ and $[44\bar{1}]_{B8}$, (Fig. 2a and 2b, respectively) are symmetry related via a mirror plane perpendicular to $\mathbf{c}_{B8}$ in the hexagonal *B*8-type structure. The *B*8-type reflections (circled in Fig. 2) are therefore in common. The satellite reflections at $\mathbf{H} = \mathbf{G}_s \pm m\mathbf{q}$, however, are not. The primary modulation-wave vector $\mathbf{q}$ is not excited in the zero-order Laue zone (or ZOLZ) in Fig. 2b, but can instead be observed in the first-order Laue zone (or FOLZ) ring. Twinned specimens like this were frequently found.

Real Space Comparison of Fe_6Ge_5 and B8-Type Structures

The close relationship between the reciprocal lattices of the *B*8- and Fe_6Ge_5-type structures strongly suggests that there must also be a close relationship in real space between the two structure types. The atomic coordinates reported for the Fe_6Ge_5 structure by Malaman *et al.* (7) (see Table 1) were used in what follows. An easy description of the Fe_6Ge_5 structure can be made by considering the structure to be built up from polyhedra of Ge atoms centred by Fe atoms. Note that this way to consider the structure is for descriptive purposes only and does not exclude other atomic interactions or imply that they are unimportant.

In the Fe_6Ge_5 structure, Fe(1) is coordinated by five Ge atoms in the form of a square pyramid, Fe(2), Fe(3), and Fe(4) are coordinated by six Ge atoms in the form of more or less distorted octahedra and Fe(5) is coordinated by seven Ge atoms in the form of a pentagonal prism. All Ge atoms belong to the $Fe(2)Ge_6$ octahedron, the $Fe(3)Ge_6$ octahedron and/or the $Fe(5)Ge_7$ pentagonal bipyramid.

TABLE 1

Atom	*x*/Å	*y*/Å	*z*/Å
Fe(1)	0.1229(4)	0	0.0153(5)
Fe(2)	0.25	0.25	0.5
Fe(3)	0	0.2533(4)	0.5
Fe(4)	0.2846(6)	0.2605(4)	0.1755(5)
Fe(5)	0.0793(5)	0.5	0.2806(6)
Ge(1)	0.3645(3)	0.0	0.0068(3)
Ge(2)	0.0451(3)	0.1970	0.2125(3)
Ge(3)	0.3420(4)	0	0.3720(5)
Ge(4)	0.3515(4)	0.5	0.4000(5)

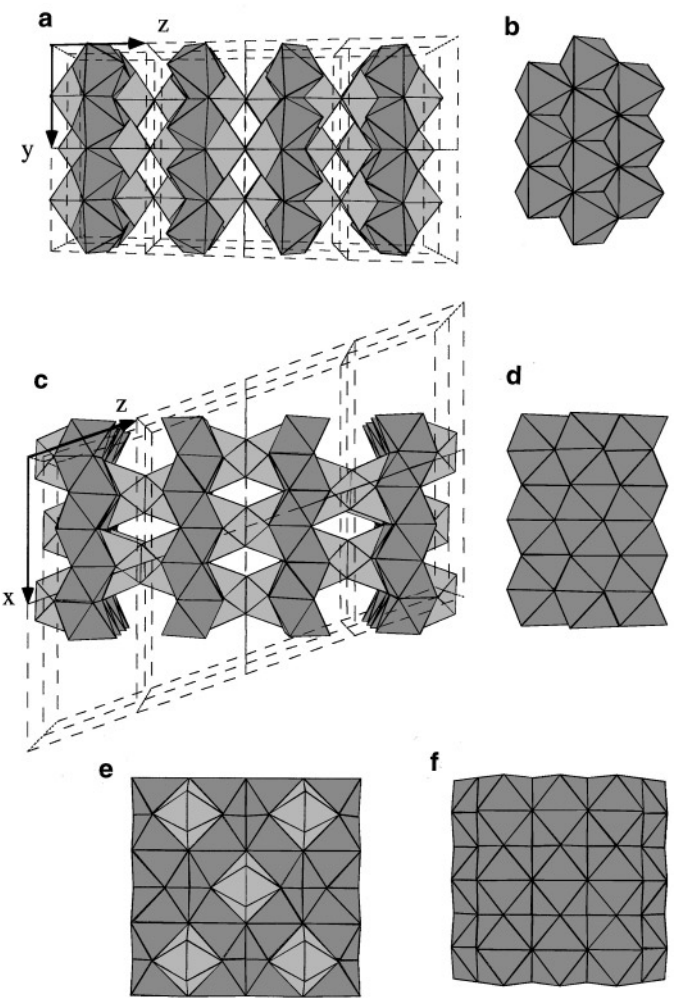

FIG. 3. (a), (c), and (e) show the crystal structure of Fe_6Ge_5 with all Ge atoms represented as vertices of polyhedra. The coordination polyhedra of Fe(2), Fe(3) (dark gray), and Fe(5) (light gray) are indicated to emphasize the relation to the *B*8-type structure. (Fe(1) and Fe(4) are not indicated, compare with Fig. 4.) The borders of the drawing are chosen in order to emphasize the orthorhombic sublattice. (a), (c), and (e) show the three orthogonal directions of Fe_6Ge_5, $\langle 100\rangle_m$, $\langle 0\bar{1}0\rangle_m$, and $\langle 104\rangle_m$, respectively, and next to them, in (b) (d), and (f), the *B*8-type structure is shown in the corresponding directions. Note, by comparing (a) and (b), how all Ge atoms except the Ge(1) at $z \approx 0$ can be described by a slab of the *B*8-type structure. Note further by comparing (c) with (d) that the heights of these octahedra slabs are shifted with respect to each other (along $\mathbf{a}_m$, i.e., $\mathbf{c}_{B8}$) in the two structures.

Figures 3a, 3c, and 3e show the crystal structure of Fe_6Ge_5 along three orthogonal directions (i.e., along (a) $[100]_m$, (c) $[010]_m$, and (e) $[104]_m$) with only these three coordination polyhedra outlined (i.e., all Ge atoms but not all Fe atoms are indicated). The octahedra are represented with a dark-gray shade while the pentagonal bipyramid (partly hidden of the octahedra) is represented with a lighter gray shade. Note that the $Fe(2)Ge_6$ and $Fe(3)Ge_6$ octahedra share faces along $[100]_m$ (corresponding to $[001]_{B8}$) and form $(001)_m$

octahedral layers or slabs perpendicular to $\mathbf{c}_m^*$ (cf. Figs. 3a and 3c).

These same slabs of octahedra are found in the *B*8-type structure forming infinite layers perpendicular to (all symmetry equivalent) $\langle 11\bar{2}0\rangle_{B8}^*$ directions. This is demonstrated in Figs. 3b, 3d, and 3f, where three projections of the *B*8-type structure ($c/a = 1.25$) are shown for comparison with Figs. 3a, 3c, and 3e. (Note again that in Fe_6Ge_5, the $Fe(2)Ge_6$ and $Fe(3)Ge_6$ octahedra are compressed along the $\mathbf{a}_m$ axis in total equivalence to the compression along the $\mathbf{c}_{B8}$ axis of the intermetallic *B*8-type structures ($c/a \approx 1.25$, see above)). By inspection of Figs. 3a–3d, it is clear that neighboring $(001)_m$ octahedral slabs in Fe_6Ge_5 are related by a pseudo-mirror plane not present in the *B*8-type structure. Formally, the $(001)_m$ octahedral array of Fe_6Ge_5 could thus be described as a twin derivative of the *B*8-type structure. The Ge(1) atoms at $z \approx 0$, however, do not belong to this twinned *hcp* array. (The apparent *xy* mirror plane in Figs. 3a and 3c relating the $(001)_m$ octahedral slabs is not a crystallographic mirror plane, *vide infra*).

An alternative way to describe the difference between the arrangements of the octahedral slabs in the two structures is to consider the relative heights (along $\mathbf{a}_m = 2\mathbf{c}_{B8}$) of the one-octahedra thick slabs in the two structure types. Comparing Figs. 3c with 3d, it is apparent that the octahedral slabs in the Fe_6Ge_5 structure are shifted relative to each other by 1/2 $\mathbf{c}_{B8}$ compared to their positions in the *B*8-type structure. This leads to a centered pseudo-orthorhombic lattice in projection down b_m and explains the $h0l, l = 2n$ condition observed on the Bragg reflections of the *B*8-type lattice (cf. Fig. 1a). However, the ordered occupancy of 1/2 of the pentagonal bipyramid lowers this symmetry to monoclinic.

By inspection of Fig. 3, it is clear that the derivation of the reciprocal lattice of the Fe_6Ge_5 structure from the *B*8 structure is justified also from real space considerations; $\mathbf{a}_m = 2\mathbf{c}_{B8}$ and $\mathbf{b}_m = -2\mathbf{b}_{B8}$ can be directly derived from the real space structure, while the relationship $\mathbf{c}_m = 2\mathbf{a}_{B8} + \mathbf{b}_{B8} - 1/2\mathbf{c}_{B8}$ includes a shift of atoms and does not have such an obvious relation to the *B*8-type structure.

Five of the Ge atoms of the $Fe(5)Ge_7$ pentagonal bipyramid (i.e., not Ge at $z \approx 0$) form a distorted trigonal bipyramid. This corresponds to the trigonal bipyramidal position in a *B*8-type structure. In intermetallic *B*8-type structures this position is (on average) partially filled and the ordering pattern of these vacancies/interstitials is the cause of the wide range of superstructures and modulated structures found in such systems. In Fe_6Ge_5, 1/2 of the possible trigonal bipyramidal positions on each side of the *B*8-type octahedra layer are filled (cf. Figs. 3e and 3f). Fe(4), cf. Fig. 4, could topologically be considered to correspond to the other trigonal bipyramidal site of the *B*8-type array, but the third Ge atom in the triangular base is missing. All atomic positions except Ge(1) and Fe(1) at $z \approx 0$ hence can be described by slabs of a *B*8-type structure shifted relative each other compared to a *B*8-type structure. Since 1/2 of the trigonal bipyramids are filled with a Fe atom in an ordered manner, these *B*8 slabs can be considered as *slabs of a B8-type superstructure.*

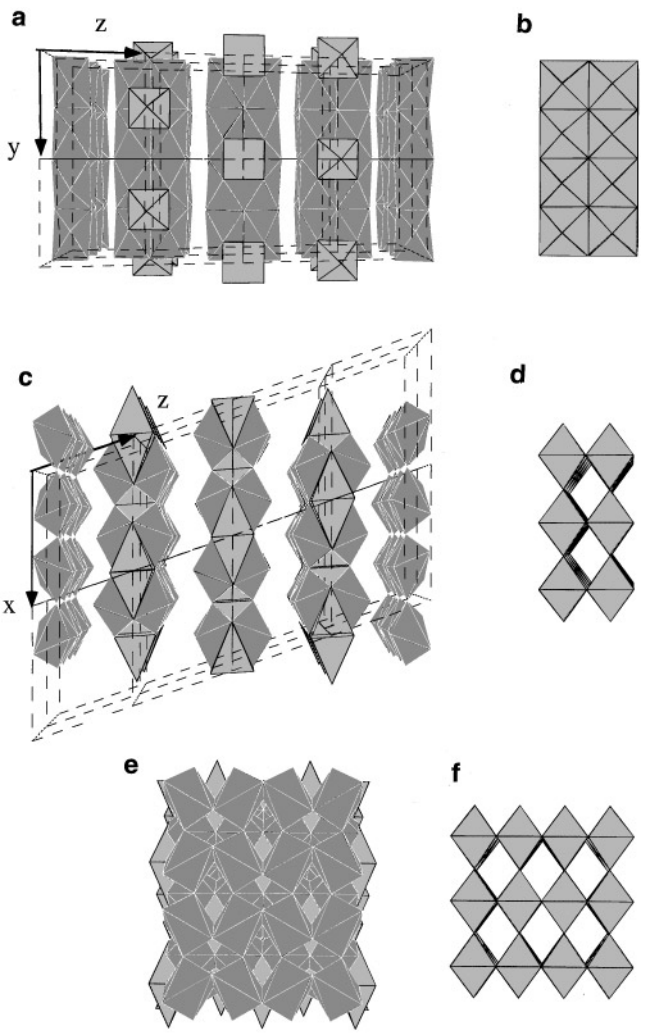

FIG. 4. (a), (c), and (e) show the crystal structure of Fe_6Ge_5 in accordance with Fig. 3. The zone axes are the same as in Figs. 3a, 3c, and 3e and all Ge atoms are again represented as vertices of polyhedra. The coordination polyhedra of Fe(1) (light gray) and Fe(4) (dark gray) are now indicated to emphasize the relation to the *B*1-type structure. Next to these drawings, in (b), (d), and (f), a two-octahedra wide slab of the *B*1-type structure in the corresponding directions is shown. Note in (a) and (b) how all Ge atoms can be described by the vertices of the octahedra in these slabs of the *B*1-type structure. Note how the elongation of the $Fe(2)_2Ge_6$ octahedra causes the distortion of the *B*1-type sublattice.

Structure Description in Terms of B8 Intergrown with B1

In addition to this description of Fe_6Ge_5 in terms of slabs of hcp Ge atoms, the structure can also be described using

slabs of ccp (cubic close packed) Ge atoms: *All* Ge atoms belong to a two-octahedra wide slab of ccp Ge atoms. All Ge atoms belong to $Fe(1)Ge_5$ square pyramid and/or the $Fe(4)Ge_6$ octahedron. Figures 4a, 4c, and 4e shows the crystal structure of Fe_6Ge_5 (in the same three orthogonal directions as in Fig. 3) with only these two coordination polyhedra outlined, while Figs. 4b, 4d, and 4f show a portion of a ccp array with some octahedral sites marked (full occupancy of all available octahedra produces the NaCl, or *B*1-type structure). The $Fe(4)Ge_6$ octahedra form a two-octahedra thick infinite slab of ccp Ge atoms, terminated with $(110)_{B1}$ planes, in which 2/3 of the octahedra are filled with Fe(4) (compare Figs. 4a and 4b). These $Fe(4)Ge_6$ octahedra share edges in the plane perpendicular to $\mathbf{a}_\mathbf{m}$ and corners along $\mathbf{a}_\mathbf{m}$. One-half of the octahedral sites in between these layers are filled with *two* Fe(1) atoms, one in each square pyramid. This results in a short Fe–Fe distance of 2.39 Å. Every second octahedron along $\langle 010 \rangle_\mathrm{m}$ rods of octahedra positions are filled with two Fe(1) atoms, cf. Fig. 4a, and every second octahedron along $\langle 100 \rangle_\mathrm{m}$ rods, cf. Fig. 4c, are filled with two Fe(1) atoms. These $Fe(1)_2Ge_6$ octahedra are as expected elongated along $\mathbf{a}_\mathbf{m}$, distorting the ccp array. Note that the relative heights of the filled octahedra in the two planes at $z = \pm 1$ are not related with a mirror plane at $z = 0$, which explains the metrically orthorhombic structure with a monoclinic space group symmetry.

The crystal structure of Fe_6Ge_5 hence can be described as an "intergrowth" of slabs of hcp and ccp Ge atoms with Fe atoms in the interstices. In the hcp array, all octahedral and 1/2 of the trigonal bipyramidal sites are occupied with Fe atoms, while in the ccp array, 5/6 of the octahedral sites are occupied with Fe atoms (Fig. 5a). The projected surfaces of the *B*8- and *B*1-type structures, marked with thick lines in Fig. 5b, are topologically identical in the two structures. This surface is in common for the *B*8 slab and the *B*1 slab in the Fe_6Ge_5 structure. The *B*8- and *B*1-type slabs are hence "intergrown" in such a way that the four Ge atoms, forming the top, bottom, and two vertices of the trigonal bipyramidal site in a hcp array are identical to the four Ge atoms forming the top, bottom, and two vertices of the square base of an octahedron in the ccp array (cf. Fig. 5b). Slabs of hcp and ccp atoms are hence intergrown in such a way that in the surface interconnecting the two slabs, the octahedra are packed without the formation of tetrahedral sites: The trigonal bipyramid from the hcp array and the two tetrahedra from the ccp array are instead merged in such a way that a pentagonal bipyramid is formed.

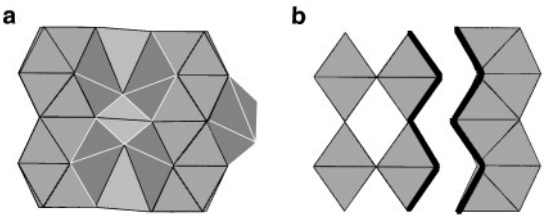

FIG. 5. In (a), a portion of the Fe_6Ge_5 structure is shown. The coordination polyhedra around Fe(1), Fe(2), Fe(3), and Fe(4) are visible. The structural intergrowth between the *B*8 and *B*1 structural motifs is illustrated in (b), where the thick lines indicate projected surfaces. These projected surfaces are topologically identical in the two structures and this surface is common for the *B*8 slab and the *B*1 slab in the Fe_6Ge_5 structure.

The result of this atomic arrangement is a very dense packing of atoms; the unit-cell volume of the Fe_6Ge_5 structure is 572.87 $Å^3$, i.e., the volume of $Fe_{2.4}Ge_2$ is 57.0 $Å^3$, while the extrapolated values for the *B*8-type structures are 68.0 (for the β phase) and 68.8 for (the η phase).

ACKNOWLEDGMENT

Financial support for A-K.L. from STINT, via the Swedish Natural Science Council (NFR), is gratefully acknowledged.

REFERENCES

1. T. B. Massalski (Ed.), "Binary Alloy Phase Diagrams," AMS, Ohio, 1986.
2. K. Kanematsu, *J. Phys. Soc. Japan* **20**(1), 36 (1965).
3. K. Kanematsu and T. Ohoyama, *J. Phys. Soc. Japan* **20**(2), 236 (1965).
4. E. Adelson and A. E. Austin, *J. Phys. Chem. Solids* **26,** 1795 (1965).
5. P. K. Panday and K. Schubert, *J. Less-Common Met.* **18,** 175 (1969).
6. B. Malaman, J. Steinmetz, and B. Roques, *J. Less-Common Met.* **75,** 155 (1980).
7. B. Malaman, M. J. Philippe, B. Roques, A. Courtois, and J. Protas, *Acta Crystallogr. B* **30,** 2081 (1974).
8. A.-K. Larsson, "Crystal Structures of Tin Intermetallics," Ph.D. thesis, University of Lund, 1994.